Mathematical Biosciences and Engineering

http://www.aimspress.com/journal/MBE

MBE, 23(1): 124–147.
DOI: 10.3934/mbe.2026006
Received: 29 July 2025
Revised: 22 October 2025
Accepted: 07 November 2025
Published: 02 December 2025

Research article

Cost-performance trade-off analysis of physicochemical phosphorus removal systems for wastewater treatment: A bi-objective optimization approach

Florencia Caro[1,*], Diego Rossit[2], Claudia Santiviago[1], Jimena Ferreira[3,4] and Sergio Nesmachnow[5]

[1] Biotechnological Processes for the Environment Group, Faculty of Engineering, Universidad de la República, Montevideo, Uruguay, 11300

[2] Department of Engineering, INMABB, Universidad Nacional del Sur (UNS)-CONICET, Bahía Blanca, Argentina, 8000

[3] Chemical & Process Systems Engineering Group, Faculty of Engineering, Universidad de la República, Montevideo, Uruguay, 11300

[4] Heterogeneous Computing Laboratory, Faculty of Engineering, Universidad de la República, Montevideo, Uruguay, 11300

[5] Universidad de la República, Uruguay

* **Correspondence:** Email: fcaro@fing.edu.uy.

Abstract: In an increasingly competitive world, industries face growing pressure to improve efficiency while meeting strict environmental and social standards. Wastewater treatment plants (WWTPs) play a key role in reducing the environmental impact of water use across industrial, agricultural, and domestic activities. This study presents a bi-objective optimization framework to support chemical dosing decisions in physicochemical phosphorus removal (PPR) systems. Using an edible-oil WWTP as a case study, two common metal salts (aluminum sulfate and ferric chloride) are compared, considering operational cost and phosphorus removal efficiency as conflicting objectives. Polynomial surrogate models enabled the integration of BioWin PPR models into the optimization problem, and the weighted sum and ε-constraint methods were used to estimate the Pareto fronts, yielding complementary solutions. The proposed framework provides a practical decision-support tool for WWTPs by revealing cost–performance trade-offs. Results show that costs escalate disproportionately: reducing effluent P from 3.0 to 1.0 mg−P/L increased costs by 114% with aluminum sulfate and 355% with ferric chloride. The framework is adaptable to different PPR systems and influent conditions.

Keywords: Bi-objective optimization; physicochemical phosphorus removal; chemical costs; chemical dosing strategies; wastewater treatment; Industry 5.0.

1. Introduction

Modern industry, under the paradigms of Industry 4.0 and 5.0, is increasingly integrating advanced digital technologies to improve efficiency, productivity, and sustainability in industrial operations [1–3]. These technologies, including the Internet of Things, Artificial Intelligence, big data, cloud computing, robotics, and advanced optimization techniques, enable real-time data acquisition, predictive maintenance, process optimization, and automation. As a result, smart industry enhances operational performance, reduces costs, and improves quality control. While Industry 4.0 prioritizes automation and efficiency through digital transformation, Industry 5.0 emphasizes human centricity and represents a vision of industry that goes beyond efficiency and productivity, focusing on addressing societal needs [4]. In essence, Industry 4.0 prioritizes operational efficiency, whereas Industry 5.0 highlights the significance of environmental responsibility, social goals, and the active role of humans in decision-making [3].

Wastewater treatment plants (WWTPs) play an important role in mitigating the environmental impacts of water use in industrial, agricultural, and domestic activities. Effective wastewater treatment is essential for meeting regulatory standards, enabling water reuse, and supporting ecosystem restoration [5]. These objectives are aligned with the United Nations Sustainable Development Goal (SDG) 6, which promotes the availability and sustainable management of water resources [6].

Among water pollutants, phosphorus is of particular concern due to its role in eutrophication [7]. Municipal and industrial wastewater discharges are among the primary sources of bioavailable phosphorus [8]; consequently, phosphorus discharge limits are becoming increasingly stringent, placing financial and operational burdens on WWTPs [9, 10]. In this context, the design and operation of cost-effective phosphorus removal systems that ensure regulatory compliance remains a major challenge.

Physicochemical phosphorus removal (PPR) using metal salts is a widely employed strategy to achieve low phosphorus concentrations, either as a standalone process or in combination with biological treatments [11–13]. Physicochemical removal involves the addition of metal salts that react with the dissolved phosphorus present in the water to form insoluble precipitates, which are subsequently removed by sedimentation or filtration. Additionally, pH adjustment, typically using sodium or potassium hydroxide, is often required alongside metal salt addition [14]. PPR has a simple configuration, consisting of a chemical dosing system and a settler or filter to separate the treated effluent from the chemical sludge [12]. A key advantage of physicochemical treatment is its operational flexibility, as phosphorus removal can be adjusted by modifying the chemical dosage [15].

Accurate chemical dosing is essential for the efficient operation of PPR systems: Underdosing can result in regulatory non-compliance, whereas overdosing not only increases chemical costs and sludge production but also may leave residual dissolved aluminum or iron in the treated effluent. Given the complexity of PPR mechanisms (e.g, adsorption, precipitation, and desorption) [12], and their dependence on influent characteristics (e.g, pH, alkalinity, and organic matter content) [16], chemical dosages are typically determined using laboratory tests, data from other WWTPs, and dosing charts. However, laboratory experiments (e.g., jar tests) are time-consuming [17], operational data from other WWTPs may not be directly transferable to a specific plant, and relying on dosing charts may lead to suboptimal dosing.

Modeling and optimization can support decision-making by enabling the systematic evaluation of chemical dosing strategies under site-specific conditions. In particular, multi-objective optimization (MOO) provides a framework to balance competing goals, such as minimizing operational costs and maximizing phosphorus removal efficiency. By identifying optimal trade-offs, MOO can facilitate the design and operation of WWTPs under economic and regulatory constraints.

Although MOO has been applied to various aspects of wastewater treatment, its specific use for optimizing PPR remains limited. Plant operators still rely on empirical dosing rules, which are often suboptimal under changing influent and regulatory conditions. This creates a significant gap, as there is a lack of systematic tools to quantitatively analyze the sensitive trade-offs between chemical costs and removal efficiency, especially when comparing different precipitating agents. The significance of this work lies in addressing this gap by providing a framework that translates complex simulation data into a practical decision-support tool. The approach enables operators to move beyond simple trial-and-error methods to a more strategic analysis, allowing direct comparison of chemical strategies, and helping anticipate the financial impact of stricter future regulations.

This study proposes a bi-objective optimization approach to evaluate and compare the performance of PPR systems using two commonly employed metal salts: Aluminum sulfate and ferric chloride. Separate simulation models were developed for each coagulant using the commercial wastewater treatment simulator BioWin. As BioWin functions as a black-box model, surrogate models were constructed to approximate the system behavior and facilitate their integration into the optimization framework. Several polynomial models were evaluated to ensure an accurate representation of the PPR system, and the weighted sum and ε-constraint methods were used to estimate the Pareto fronts. The WWTP of an edible oil production company, where PPR is employed to supplement biological processes to meet stringent discharge limits, is used as a case study. The proposed framework enables a cost-performance trade-off analysis of alternative dosing strategies, providing a practical decision-support tool for wastewater treatment, addressing operational efficiency and effluent quality.

The remainder of this paper is organized as follows: Section 2 reviews relevant literature on the application of MOO in wastewater treatment and compares the main approaches used. Section 3 presents the general multi-objective optimization framework, details the industrial case study, and describes the formulation of the optimization problem and the development of surrogate models. Section 4 presents and discusses the results of the cost-performance analysis for each chemical agent. Finally, Section 5 summarizes the main findings and conclusions. This article is an extended version of the work presented at the 7th Ibero-American Congress of Smart Cities (ICSC-CITIES 2024) and published in its proceedings [18].

2. Literature review

Recent studies have increasingly explored MOO approaches for improving the design and operation of WWTPs. These contributions differ in the optimization objectives, computational techniques, and the level of integration with process simulators or control systems. Table 1 summarizes representative works, highlighting their objectives, optimization methods, main findings, and limitations.

Padrón et al. [19] propose a sustainable WWTP design framework using MOO, where total cost, energy consumption, and reclaimed wastewater are considered sustainability metrics. A hybrid approach that combines lexicographic and ε-constraint methods is used to estimate the Pareto front, and a modi-

fied technique for order of preference by similarity to ideal solution (M-TOPSIS) analysis is employed to find the best trade-off solution. Similarly, Hakanen et al. [20] present an interactive MOO approach for WWTP design and operation that integrates a commercial wastewater treatment simulator with a MOO tool. The approach is applied to a case study that seeks to minimize effluent total nitrogen and operational costs, considering four cost components. Compared to traditional non-iterative methods, the proposed approach improves problem formulation and helps decision-makers understand trade-offs between conflicting objectives.

For control applications, Han et al. [21] propose a multi-objective integrated optimal control (MIOC) strategy that combines optimization and control into a unified framework. The method minimizes a comprehensive cost function that accounts for both operational performance and tracking accuracy. A multi-gradient algorithm is used to determine dynamic set-points and control actions that balance conflicting objectives, which include effluent quality, energy consumption, and errors of controlled variables. Tests on Benchmark Simulation Model No. 1 (BSM1) show that the MIOC approach yields superior results in terms of solution quality and energy cost, avoiding the fluctuations in set points that can arise when optimization and control are handled independently.

Another approach presented by Zhang & Yong [22] involves a dynamic optimization control method that combines a neural network-based prediction model with the multi-objective dragonfly algorithm (MODA). The neural network predicts effluent quality and energy consumption, which serves as the objective function for optimization. The MODA is then used to determine the optimal set points for dissolved oxygen and nitrate nitrogen concentrations. Tests on BSM1 demonstrate that this method effectively identifies and tracks optimal set points, ensuring effluent quality and significantly reducing energy consumption.

Qiao et al. [23] apply an intelligent multi-objective optimal control strategy (IMOOC) based on an adaptive differential evolution algorithm (Adaptive DE) to optimize and control dissolved oxygen and nitrate nitrogen concentrations. The algorithm minimizes aeration energy and effluent quality indices. A two-layer hierarchical control architecture is used, where the upper layer optimizes set points and the lower layer uses controllers to minimize the error. Tests on BSM1 under different weather conditions showed that the IMOOC can maintain effluent quality within limits and achieves better performance than other controllers in terms of environmental, economic, and technical criteria.

Genetic algorithms have also been used to determine optimal controller parameters for biological WWTPs [24]. The approach by Tejaswini et al. [24] aims to improve effluent quality while minimizing operational costs. Different objective functions, including effluent quality and operational cost indices, as well as the integral square error for controller design, are considered. Tests on BSM1 show that controllers tuned using this method enhance WWTP performance compared to single-objective optimization approaches.

To support decision making in WWTP operations Liu et al. [25] propose a MOO framework that integrates interpretable machine learning models. The approach uses Extreme Gradient Boosting (XGB) models with Bayesian optimization to predict effluent quality and energy consumption based on influent conditions and operational parameters. The Non-dominated Sorting Genetic Algorithm II (NSGA-II) is used to solve the MOO problem, and TOPSIS is used to select operational parameters. The applicability of the framework is demonstrated using BSM1, showing that it effectively captures the complex non-linearity of the wastewater treatment process. NSGA-II and TOPSIS efficiently determine ideal operating parameters, enabling energy consumption reduction while ensuring effluent quality under

multiple influent conditions.

Overall, these studies demonstrate that MOO effectively balances effluent quality and operational cost, yet they vary considerably in scope and methodology. Design-oriented frameworks, such as [19, 20], emphasize static optimization, while control-oriented ones [21–23] incorporate dynamic and real-time process regulation. Machine learning–based approaches [22, 25] improve predictive capacity but require extensive datasets and often lack interpretability. Evolutionary algorithms, such as NSGA-II or MODA, provide flexibility and robustness but demand high computational effort and parameter tuning.

In contrast, the present study focuses on PPR, a process that has received little attention in MOO research. PPR involves strong nonlinearities caused by chemical precipitation reactions, which complicate direct optimization. To overcome this challenge, surrogate modeling is introduced to integrate detailed mechanistic simulators like BioWin within an optimization framework. To the best of the authors knowledge, the first application of a MOO framework to analyze and improve PPR was presented in our previous conference work [18]. This article extends the previous work by incorporating updated BioWin simulation models, providing a more detailed description of the surrogate model construction process, and applying the framework to compare the performance of two metal salts for PPR.

Table 1. Summary of representative studies applying multi-objective optimization to wastewater treatment processes.

Reference	Application	Objectives	Optimization Method	Main Findings / Limitations
Padrón et al. [19]	WWTP design	Cost, energy, water reuse	ε-constraint and TOPSIS	Good sustainability trade-offs; static design only.
Hakanen et al. [20]	WWTP design/operation	N removal, cost	Interactive MOO	Improved decision understanding; limited scalability.
Han et al. [21]	Control	Effluent quality, energy, error	MIOC	Real-time control; high model complexity.
Zhang & Yong [22]	Control	Effluent quality, energy	MODA	Accurate; data-intensive.
Qiao et al. [23]	Control	Effluent quality, energy	Adaptive DE	Robust; computationally heavy.
Tejaswini et al. [24]	Control	Effluent quality, cost, error	Genetic algorithms	Enhanced performance; computationally intensive.
Liu et al. [25]	Operation	Effluent quality, energy	NSGA-II + TOPSIS	Good accuracy; interpretability issues.
This article	PPR operation	Cost, P removal	Weighted sum / ε-constraint	First systematic MOO for PPR.

3. Methodology

This section describes the adopted methodology, including the general MOO framework, problem description, mathematical formulation, and surrogate model development.

3.1. Multi-objective optimization

MOO provides a framework for identifying a set of optimal solutions, known as the Pareto front or non-dominated solutions, that represent the inherent trade-offs between conflicting objectives. Several methods exist to estimate the Pareto front, including the weighted sum, ε-constraint, hybrid methods, lexicographic ordering, goal programming [26], and evolutionary algorithms [27]. The weighted sum and ε-constraint methods used in this work are described in more detail below.

3.1.1. Weighted sum

The weighted sum method transforms the MOO problem into a single-objective one by assigning a weight to each objective function k and minimizing their weighted sum [26]. The weighting coefficients w_k are positive real numbers that satisfy $\sum w_k = 1$. Because the objectives usually have different magnitudes, normalization is required prior to aggregation to ensure that the weights reflect the relative importance of each objective accurately [28]. Normalization can be performed using the ideal (best values for each objective) and anti-ideal (worst values for each objective) values, which are obtained by evaluating the objective functions at their extreme solutions.

Extreme solutions of the Pareto front can be estimated using single-objective and lexicographic optimization. In single-objective optimization, each objective is optimized individually to approximate the extremes, but this does not guarantee non-dominated solutions. Lexicographic optimization addresses this limitation by optimizing one objective first, then the second, while enforcing the optimal value of the first [26]. By switching the order of priority between the objectives the extremes of the front can be obtained.

If the problem is convex, any Pareto-optimal solution can be found using the weighted sum method [26]. However, different weight combinations may yield the same solution, and so a uniform sampling of weights does not guarantee a uniform distribution of solutions along the front. Additionally, this method cannot capture unsupported Pareto-optimal solutions in non-convex regions of the front [26]. Despite these limitations, the weighted sum method remains widely used due to its simplicity [29].

3.1.2. ε-constraint

The ε-constraint method also transforms the MOO problem into a single-objective one, but instead of aggregating the objectives, it optimizes one objective while converting the others into inequality constraints with upper or lower bounds ε_k depending on whether they are to be minimized or maximized [26]. The solutions of the Pareto front are obtained by varying the value of the bounds [30]. Unlike the weighted sum method, this approach can identify Pareto-optimal solutions even in non-convex regions of the front [26]. However, the method introduces additional constraints to the original problem, potentially making it more difficult to solve.

3.1.3. Performance metrics

Evaluating the performance of MOO methods involves assessing three key aspects: Cardinality (i.e., number of non-dominated points generated), solution quality (i.e., proximity to the true Pareto front), and diversity (i.e., distribution and coverage of solutions) [31, 32]. Several metrics have been proposed to assess the quality of a Pareto front approximation [33]. Spacing, spread, and hypervolume metrics used in this work are described below.

Spacing is a diversity metric that evaluates how uniformly distributed the non-dominated solutions are. A value of 0 indicates that the solutions are evenly spaced across the Pareto front. However, this metric does not account for the coverage of the Pareto front, as it does not consider proximity to the extreme solutions. Spacing is computed using Eq. (3.1), based on the formulation by Schott [34]:

$$\text{spacing} = \sum_{i=1}^{m} \left| d_i - \bar{d} \right|, \tag{3.1}$$

where m is the number of non-dominated solutions, d_i is the minimal distance between solution i and its nearest neighbor, and $\bar{d}$ is the average of these distances.

Spread expands upon the spacing metric by incorporating information about the extent of the Pareto front. In addition to evaluating the distribution of solutions, it considers their proximity to the extreme points, thereby accounting for uniformity and coverage. This metric is calculated using Eq. (3.2), as proposed by Deb [35]:

$$\text{spread} = \frac{\sum_{k=1}^{OF} d_k^e + \sum_{i=1}^{m} |d_i - \bar{d}|}{\sum_{k=1}^{OF} d_k^e + m\bar{d}}, \tag{3.2}$$

where OF is the number of objective functions, and d_k^e is the distance between the extreme point of the front for the k-th objective and the nearest non-dominated solution.

Hypervolume quantifies proximity and diversity. It measures the volume enclosed between the Pareto front and a reference point [33], typically the anti-ideal vector, ensuring that only non-dominated solutions contribute positively to the metric. A higher hypervolume value indicates better overall performance, reflecting proximity to the true Pareto front and good distribution of solutions.

3.2. Problem description

The WWTP of an edible oil production company is used as a case study. The company operates its own WWTP and supplements biological wastewater treatment with PPR to comply with phosphorus discharge limits before discharging the effluent into a nearby watercourse. The raw effluent contains elevated concentrations of inorganic phosphorus due to the use of phosphoric acid in the oil refining process.

A simplified block diagram of the WWTP is shown in Figure 1. The system consists of a homogenization tank (HT), followed by a dissolved air flotation (DAF) unit for fat and suspended solids removal, and an extended aeration (EA) system for organic matter degradation. After this treatment, the effluent meets all national discharge standards [36], except for phosphorus (Table 2). PPR with metal salts is used as an additional treatment, and sodium hydroxide (NaOH) is added for pH control. Both reagents are dosed directly into the pipe at the outlet of the secondary settler, and the resulting chemical sludge is separated from the treated effluent in a tertiary settler. The pipe and the tertiary settler dimensions are detailed in Figure 1, and these design features influence the efficiency of phosphorus removal.

Achieving lower phosphorus concentrations typically requires higher chemical dosages, increasing operational costs. This trade-off becomes especially relevant as regulatory discharge limits become more stringent. Understanding this balance can help anticipate future compliance costs and identify cost-effective dosing strategies. In this study, two commonly used metal salts are compared: Aluminum

sulfate ($Al_2(SO_4)_3$) and ferric chloride ($FeCl_3$). Bi-objective optimization is used to evaluate the trade-off between operational costs and phosphorus removal, two inherently conflicting objectives.

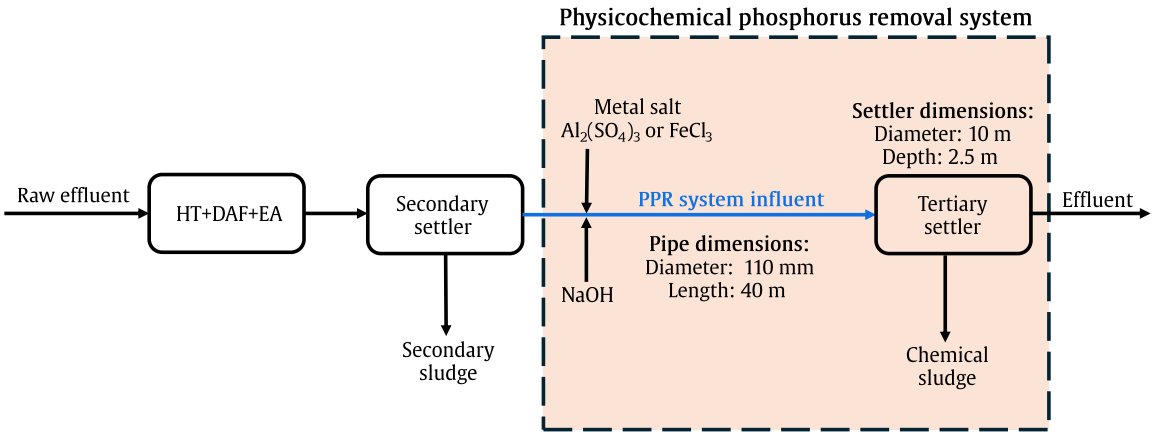

Figure 1. Simplified diagram of the edible oil WWTP.

Table 2. Influent parameters at the inlet of the PPR system of the edible oil WWTP used as a case study.

Influent parameter	Value
Flow (m^3/d)	1000
Total phosphorus (mg−P/L)	17
pH	7.4
Total Kjeldahl Nitrogen (mg−N/L)	4
Nitrate (mg−N/L)	1.5
Alkalinity (mg/L)	80
Inorganic suspended solids (mg/L)	2
Soluble calcium (mg/L)	160
Soluble magnesium (mg/L)	60

3.3. Mathematical formulation

The formulation of the bi-objective optimization problem has the following general form:

$$\min_{x_1,x_2} \quad \begin{bmatrix} C(x_1,x_2) \\ TPc(x_1,x_2) \end{bmatrix} \tag{1a}$$

$$\text{s.t.} \quad 0 \le TPc(x_1,x_2) \le 5 \tag{1b}$$

$$6 \leq pH(x_1, x_2) \leq 9 \tag{1c}$$

$$TPc(x_1, x_2) = f(x_1, x_2) \tag{1d}$$

$$pH(x_1, x_2) = g(x_1, x_2) \tag{1e}$$

The objective is to simultaneously minimize the operational cost (C) and the phosphorus concentration after PPR (TPc), subject to phosphorus and pH discharge limits (Eq. 1b and Eq. 1c) and the PPR system's model (Eq. 1d and Eq. 1e). The decision variables are the daily dosages of metal salt (x_1), either aluminum sulfate (8 wt % Al_2O_3) or ferric chloride (40 wt %), and sodium hydroxide solution 5 mol/L (x_2) used for pH control. The cost function is expressed in USD/d, phosphorus concentration in mg−P/L, and chemical dosages in L/d.

The cost function considers only chemical costs and is defined as:

$$C(x_1, x_2) = \alpha x_1 + \beta x_2, \tag{4}$$

where α and β are the unit costs (USD/L) of the metal salt and sodium hydroxide, respectively. Local market prices are used to calculate α and β : 330 USD/t for aluminum sulfate (8 wt % Al_2O_3) [37], 555 USD/t for ferric chloride (40 wt %) [38], and 980 USD/t for sodium hydroxide flakes (70 wt%) [38]. The corresponding unit costs α and β are:

- Aluminum sulfate solution: 0.43 USD/L (density: 1300 g/L [37])
- Ferric chloride solution: 0.80 USD/L (density: 1420 g/L [38])
- Sodium hydroxide solution 5 mol/L: 0.28 USD/L

The PPR system's model (Eq. 1d and Eq. 1e) defines the relationship between the chemical dosages (metal salt and sodium hydroxide) and the effluent parameters (phosphorus concentration and pH) after the physicochemical treatment for a given set of influent characteristics (Table 2). BioWin, a widely used commercial simulator for modeling wastewater treatment processes, has one of the most up-to-date mechanistic models for chemical phosphorus removal [39] and has been employed to simulate PPR in municipal and industrial WWTPs [40,41]. However, BioWin is a sequential modular simulator and functions as a black box, which limits the direct integration of its internal models into equation-oriented optimization frameworks. A surrogate model built from BioWin simulation data is proposed to represent the PPR system and enable the integration of BioWin models into the optimization framework.

3.4. Surrogate model construction

The construction of the BioWin surrogate models involves four main steps: Modeling the PPR system in BioWin, generating simulation data, fitting the data, and validating the model. These steps are carried out for two scenarios: One using aluminum sulfate (Al scenario) and the other using ferric chloride (Fe scenario) as the precipitating agent. The work is conducted in Python and BioWin, on a device with an AMD Ryzen 7 5700U processor, 16.0 GB of RAM, and Windows 11.

3.4.1. BioWin model

The physicochemical system is modeled in BioWin 6.3. Table 3 summarizes the selected model options for the Al and Fe scenarios, respectively, along with a brief justification for each choice. The

operating temperature is set to 17 °C, which corresponds to the average annual temperature at the WWTP's location [42].

The system layout implemented in BioWin is shown in Figure 2. The influent is defined using the *COD Influent* block, with the influent parameters listed in Table 2. For the influent wastewater fractions, the option *typical wastewater fraction values for settled effluent* is selected, as the influent to the PPR system comes from a secondary settler. Given that most of the phosphorus in the influent is dissolved, the soluble phosphate to total phosphorus fraction is set to 0.99. Additionally, the default P/COD and N/COD ratios for the unbiodegradable COD are set to 0. This adjustment is necessary because influent COD is significantly higher than phosphorus concentration, and using the default ratios would result in an overestimation of total phosphorus. Specifically, the model would assign more phosphorus to the unbiodegradable COD fraction than is actually present, triggering a total phosphorus mass balance error.

The pipe where chemicals are dosed is modeled using the *Plug flow channel* block, specifying the length and diameter. The settler is modeled using the *Ideal clarifier* block, specifying its area and depth. Additional details on the BioWin model are provided in the Supplementary Material.

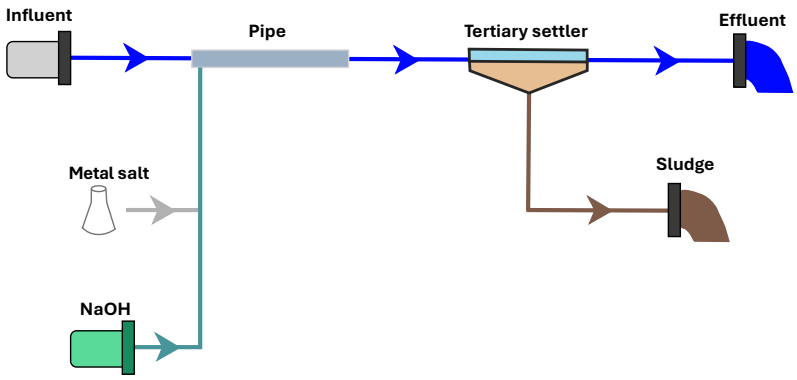

Figure 2. Diagram of the PPR system, adapted from BioWin.

3.4.2. Data acquisition

The data acquisition process involves running multiple BioWin simulations with varying dosages of metal salt and sodium hydroxide. Sampling ranges for the chemical dosages are defined based on a preliminary analysis, considering metal salt-to-phosphorus molar ratios recommended in the literature [12, 43]. The selected intervals are then checked to ensure that they adequately cover the range of interest, particularly with respect to national discharge standards [36]. Dosage values are randomly sampled within the defined intervals to generate the simulation dataset. A total of 500 simulations are performed for the Al scenario and 1000 for the Fe scenario. The larger number of simulations in the latter case is due to the broader dosage range for the Fe scenario. Preliminary simulations indicate that achieving low phosphorus concentrations with ferric chloride requires significantly higher dosages of ferric chloride and sodium hydroxide. Therefore, a denser sampling is needed to properly capture the

Table 3. Model options for BioWin simulation of the PPR system.

Model option	Description	Reasons	Scenario*	
			Al	Fe
Use BioWin integrated ASDM model	Activated Sludge/Anaerobic Digestion model, chemical equilibrium, precipitation, pH module	Includes physicochemical model	x	x
Include pH calculations	Otherwise pH of 7.0 is assumed	pH affects phosphorus removal efficiency [15]	x	x
Apply pH limitation in kinetic equations	Considers pH influence in kinetic rates, gas-liquid mass transfer, and precipitation reactions	pH affects phosphorus removal efficiency [15]	x	x
Include precipitation reactions for struvite, brushite, and apatite	Models chemical phosphorus precipitation reactions	Influent contains calcium and magnesium	x	x
Include precipitation reactions for calcium hydroxide	Models chemical phosphorus precipitation reactions	Influent contains calcium	x	x
Include precipitation reactions for calcium carbonate	Models chemical phosphorus precipitation reactions	Influent contains calcium	x	x
Include precipitation reactions for magnesium hydroxide	Models chemical phosphorus precipitation reactions	Influent contains magnesium	x	x
Include metal salt-colloidal material coagulation reactions	COD will compete with $H_2PO_4^-$ for active surface sites on the hydrated metal oxide	Organic matter affects phosphorus removal efficiency [15]	x	x
Include aluminum-phosphate adsorption/precipitation reactions	Models chemical phosphorus precipitation reactions with aluminum	Aluminum sulfate is used as the precipitating agent	x	
Include ferric-phosphate adsorption/precipitation reactions. Include iron reduction/oxidation reactions. Include vivianite and FeS precipitation/dissolution reactions	Models chemical phosphorus precipitation reactions with ferric iron	Ferric chloride is used as the precipitating agent		x

* A cross (x) indicates the selected option for each scenario.

behavior of the system across the input space. The data acquisition procedure is summarized in Algorithm 1. Steps 5 to 7 are automated using Bio2Py [44], an API developed to run BioWin using Python. More details on Bio2Py and the data acquisition process can be found at the Bio2Py repository.

3.4.3. Data fitting

Polynomial regression is used to approximate the relationship between chemical dosages and effluent characteristics after PPR. For each scenario, phosphorus concentration and pH are modeled as functions of metal salt and sodium hydroxide dosages using polynomials of degree 1 to 5. The best-fitting model is selected based on the coefficient of determination (R^2), root mean square error (RMSE), and visual inspection. A trade-off between accuracy and simplicity is considered when selecting the final polynomial degree, favoring lower-degree models when performance differences are marginal, as higher-degree models may introduce unnecessary complexity and pose challenges for subsequent optimization. Specifically, lower-degree polynomials are preferred when they provide a sufficiently accurate fit, as indicated by minimal differences in R^2 and RMSE compared to higher-degree models. All regressions are performed using Python's Scikit-learn library.

Algorithm 1 Data generation with BioWin for the Al and Fe* scenarios.

1: Initialize an empty structure -DataFrame in Python- to store the simulation results.
2: Define the number of simulations to be conducted: 500 (1000).
3: Randomly select dosages for aluminum sulfate (ferric chloride) within the interval [230, 1100] L/d ([270, 2000]) and for sodium hydroxide within the interval [0, 1000] L/d ([220, 3900]).
4: **for** each selected dosage combination **do**
5: Load the selected dosages in BioWin.
6: Run the simulation in BioWin.
7: Save the simulation results -TPc and pH- along with the corresponding chemical dosages.
8: **end for**
*The specifications for the Fe scenario are indicated in parentheses.

3.4.4. Validation

The surrogate model is validated by comparing its predictions with outputs from new BioWin simulations using the optimized chemical dosages. A summary of the validation procedure is shown in Figure 3. First, the optimized chemical dosages (x_1, x_2) obtained from the estimated Pareto fronts are used as inputs in new BioWin simulations. These simulations provide the effluent total phosphorus concentration and pH after PPR, denoted as TPc_{BioWin} and pH_{BioWin}, respectively. BioWin results are then compared to the corresponding surrogate model predictions for the same dosages: TPc and pH. The validation focuses on quantifying the prediction error of the surrogate model. For each solution on the Pareto front, the errors are calculated as:

$$Error_{TPc} = TPc_{BioWin} - TPc, \tag{5}$$

$$Error_{pH} = pH_{BioWin} - pH, \tag{6}$$

The errors are plotted as functions of TPc and pH, respectively, to evaluate the surrogate model's accuracy across the objective space. A positive error indicates that the surrogate model underestimates the corresponding output variable (phosphorus concentration or pH) compared to BioWin.

3.5. Solution strategy: Bi-objective optimization

In this work, *a posteriori* methods are used to solve the bi-objective optimization problem and explore the trade-offs between the objectives (Eq. 1a). To approximate the Pareto fronts, the weighted sum and the ε-constraint methods are employed, considering 20 w_i or ε values, respectively.

In the weighted sum method, the original bi-objective problem (Eq. 1a) is transformed into the normalized single-objective problem presented in Eq. 7a. Normalization is performed using the ideal ($[TPc_{\text{ideal}}, C_{\text{ideal}}]$) and anti-ideal ($[TPc_{\text{anti}}, C_{\text{anti}}]$) values of the objectives.

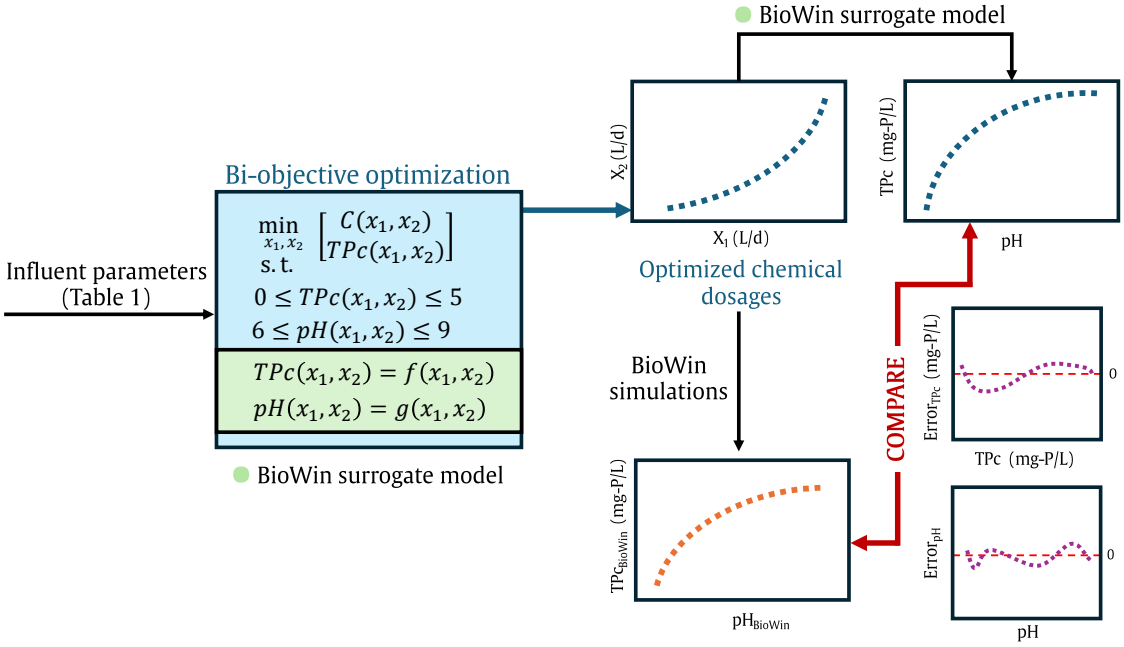

Figure 3. Summary of the surrogate model validation outline.

$$\min_{x_1,x_2} \quad \left(\frac{C(x_1,x_2)-C_{\text{ideal}}}{C_{\text{anti}}-C_{\text{ideal}}}w_1 + \frac{TPc(x_1,x_2)-TPc_{\text{ideal}}}{TPc_{\text{anti}}-TPc_{\text{ideal}}}w_2\right) \tag{7a}$$

$$\text{s.t.} \quad 0 \le TPc(x_1,x_2) \le 5, \tag{1b}$$

$$6 \le pH(x_1,x_2) \le 9, \tag{1c}$$

$$TPc(x_1,x_2) = f(x_1,x_2), \tag{1d}$$

$$pH(x_1,x_2) = g(x_1,x_2) \tag{1e}$$

where $0 \le w_i \le 1$ for i=1,2 and $w_1 + w_2 = 1$. The extreme solutions of the Pareto front are estimated using single-objective and lexicographic optimization.

For the ε-constraint method, the cost function is selected as the objective, and phosphorus concentration is added as a constraint. Parameter ε is varied within the range defined by the ideal and anti-ideal phosphorus values, resulting in the following single-objective problem:

$$\min_{x_1,x_2} \quad C(x_1,x_2) \tag{8a}$$

$$\text{s.t.} \quad TPc(x_1,x_2) \le \varepsilon, \tag{8b}$$

$$0 \le TPc(x_1,x_2) \le 5, \tag{1b}$$

$$6 \le pH(x_1,x_2) \le 9, \tag{1c}$$

$$TPc(x_1,x_2) = f(x_1,x_2), \tag{1d}$$

$$pH(x_1,x_2) = g(x_1,x_2) \tag{1e}$$

The optimization problems are formulated using Pyomo [45], a Python-based open-source modeling language for optimization, and solved with IPOPT [46], a nonlinear optimization solver. The quality of

the resulting Pareto fronts is evaluated using the number of non-dominated solutions, spacing, spread, hypervolume metrics, and computation time. The hypervolume is computed with the *hypervolume* function from the Pymoo library [47], using the anti-ideal vector ($[TPc_{\text{anti}}, C_{\text{anti}}]$) as the reference point.

Finally, the estimated Pareto fronts are used to compare the cost-performance trade-offs of aluminum sulfate and ferric chloride as precipitating agents.

4. Results and discussion

4.1. Physicochemical phosphorus removal system surrogate model

Figure 4 presents the BioWin simulation results for the Al and Fe scenarios, showing the nonlinear behavior of the PPR model. The selected chemical dosing ranges successfully capture the region of interest, as the resulting phosphorus (TPc) and pH (pH) values include those that meet discharge limits. This confirms that the dosing intervals used in the simulations were appropriate. Otherwise, if the simulations had failed to produce feasible outcomes, the dosage ranges would have required adjustment.

The simulation data span a much broader range than the region constrained by discharge requirements. Fitting a surrogate model over the entire dataset would unnecessarily increase complexity and reduce accuracy within the relevant range. To simplify the model and enable the use of lower-degree polynomials to fit the data, the surrogate is trained only on the subset of data that falls near the compliance region. Specifically, data points with phosphorus concentrations between 0 and 5.5 mg−P/L and pH values between 5.5 and 9.5 are used to fit the model, as marked in red in Figure 4.

Table 4 presents the performance metrics (R^2 and RMSE) of polynomial regression models used to approximate effluent phosphorus and pH as functions of chemical dosages. For pH, a first-degree polynomial provides a highly accurate approximation, with R^2 values of 0.99 in both scenarios and a RMSE of 0.060 and 0.045 for the Al and Fe scenarios, respectively, indicating a nearly linear relationship for pH in the selected domain. This level of accuracy is considered sufficient and, therefore a first-degree polynomial is used to represent pH. In contrast, the phosphorus concentration exhibits a more complex, nonlinear behavior, requiring higher-degree polynomials to achieve a good fit.

As an initial approach, second-degree polynomials are selected to represent phosphorus concentration in both scenarios, based on R^2 values of 0.96 and 0.97 for the Al and Fe scenarios, respectively. However, when the Pareto fronts are estimated using these models and validated against BioWin simulations, discrepancies in phosphorus concentration of up to 1.75 mg−P/L for the Al scenario and 5.5 mg−P/L for the Fe scenario are observed in the most extreme points of the front (Figure 5). This level of error is unacceptable, as a positive deviation of more than 1 mg−P/L implies that the estimated dosage would be insufficient to meet discharge limits, potentially leading to regulatory noncompliance. To improve accuracy, fourth-degree polynomials are tested for phosphorus in both scenarios based on RMSE values (0.035 and 0.037 for Al and Fe Scenarios, respectively). These polynomials significantly reduce the validation error, with a maximum deviation of 0.3 mg−P/L, considered acceptable in this context (Figure 5). On the other hand, pH errors are negligible in both cases, but show further improvement when using fourth-degree polynomials for phosphorus concentration.

The choice of polynomial degree for each output variable balances model simplicity and predictive accuracy. pH exhibits a nearly linear trend within the domain of interest, making a first-degree

polynomial sufficient, while phosphorus concentration shows more complex, nonlinear behavior that requires a fourth-degree polynomial to ensure accurate prediction of effluent levels. As a result, the final surrogate model consists of a first-degree polynomial for pH and a fourth-degree polynomial for phosphorus concentration in both scenarios.

Note that the polynomial surrogate models are trained on data near the compliance region to ensure high accuracy where it is most relevant for decision-making. Consequently, the models may not accurately capture nonlinearities outside this region, and their predictive performance in distant operating conditions could be limited. If the framework were to be applied to scenarios far from compliance, higher-degree polynomials or other surrogate models might be needed to capture the broader nonlinear behavior.

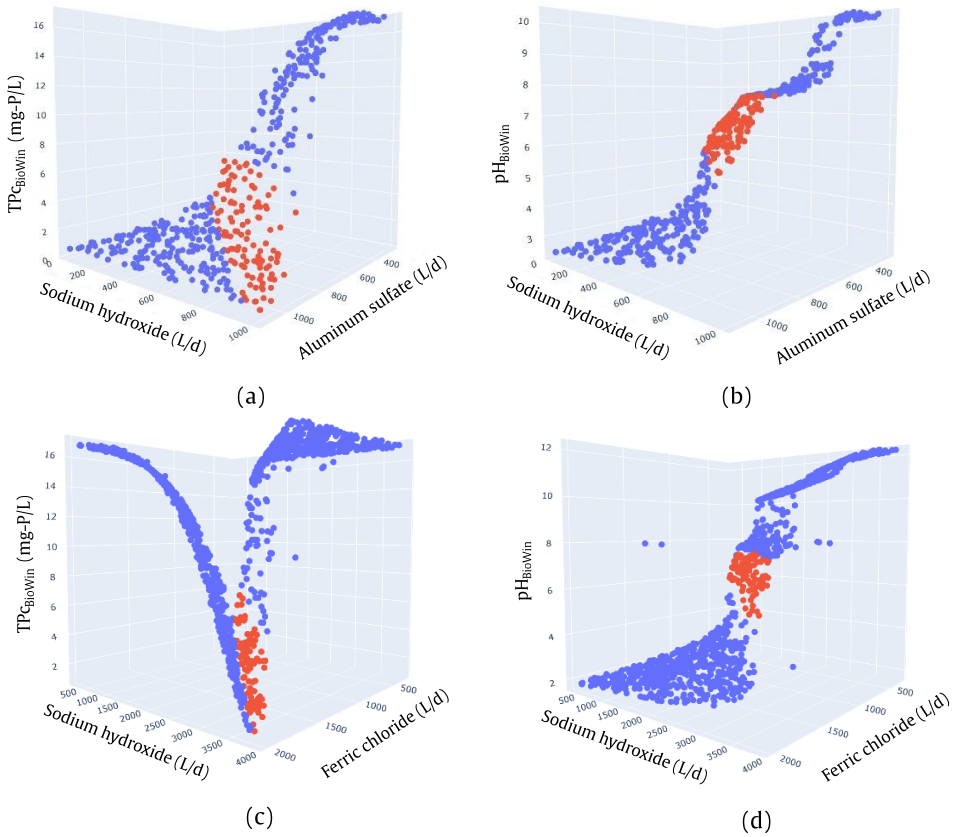

Figure 4. BioWin simulation results for Al (a–b) and Fe (c–d) scenarios. Red markers indicate the subset of data selected to fit the PPR surrogate models.

4.2. Bi-objective optimization

The estimated fronts for both scenarios and methods are shown in Figure 6, and the corresponding performance metrics are presented in Table 5. In both scenarios, the ε-constraint method yields a more uniform distribution of solutions for higher phosphorus concentrations but fails to find points near the extreme corresponding to the lowest phosphorus levels. In contrast, the weighted sum method provides more solutions in the low-phosphorus region, although fewer solutions are found in the high-phosphorus region. Overall, in this case study, the weighted sum method results in slightly better-

Table 4. Performance metrics (R^2 and RMSE) for polynomial regression models used to build the PPR surrogate models.

Degree of the polynomial	Al Scenario				Fe Scenario			
	P		pH		P		pH	
	R^2	RMSE	R^2	RMSE	R^2	RMSE	R^2	RMSE
1	0.813	0.648	0.989	0.060	0.763	0.552	0.993	0.045
2	0.963	0.285	0.993	0.048	0.966	0.209	0.996	0.032
3	0.995	0.103	0.994	0.044	0.995	0.079	0.999	0.011
4	0.999	0.035	0.999	0.019	0.999	0.037	0.999	0.005
5	0.999	0.018	0.999	0.014	0.999	0.018	0.999	0.006

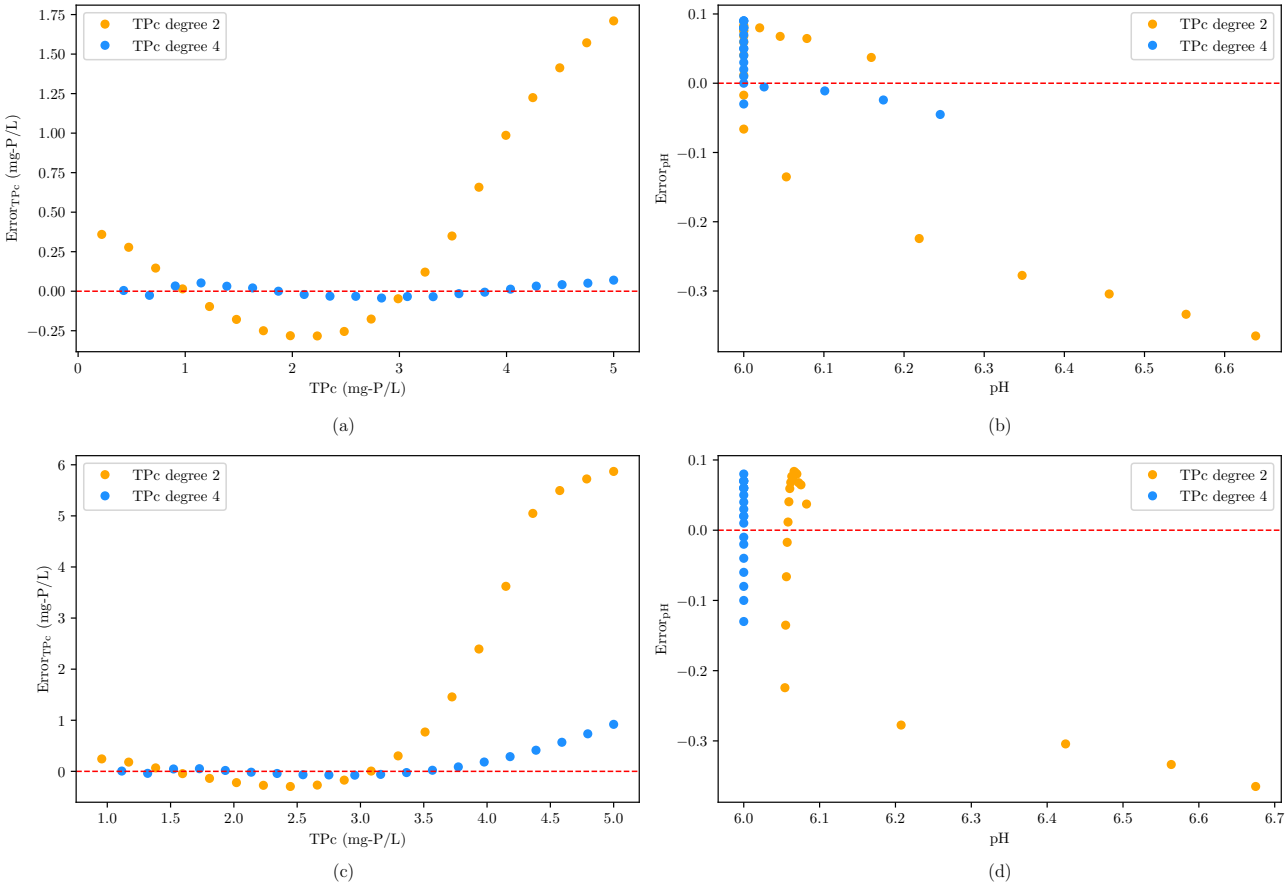

Figure 5. Validation errors for the Al (a–b) and Fe (c–d) scenarios using second- and fourth-degree polynomials to represent total phosphorus after PPR.

distributed Pareto fronts, as indicated by lower spread and spacing metrics. However, the hypervolume for the ε-constraint method is marginally higher, suggesting a slightly better approximation of the true Pareto front in terms of objective space coverage.

In this case study, the selection of the most suitable method for Pareto front estimation is not straightforward, as it depends on the specific region of interest of the decision-maker. If the priority is to identify solutions near the discharge limit, the ε-constraint method is more suitable. Conversely, if

the focus is on minimizing phosphorus concentration, the weighted sum method may be more appropriate. In any case, both methods estimate similar fronts, as reflected in their comparable hypervolume values. Computing time is also similar, on the order of 1 s, for both methods and scenarios, and does not represent a deciding factor when choosing between methods.

The weighted sum method is computationally simpler and well-suited for problems with smooth, convex Pareto fronts like the one obtained here, but it may overlook non-convex regions of the trade-off space. In this case, since the Pareto front is convex, this limitation is not a concern. However, we observe that uniformly sampling the weights does not lead to a uniform distribution of solutions along the front. On the other hand, the ε-constraint method can identify Pareto-optimal solutions even in non-convex regions of the front, but can potentially be more computationally demanding due to the additional constraints it introduces. For this case study, both methods exhibit similar computation time, indicating that the ε-constraint formulation was not significantly more expensive to solve. Overall, the methods provide complementary insights for this problem: The weighted sum efficiently explores low-phosphorus, cost-intensive solutions, whereas the ε-constraint method ensures better coverage near current discharge limits.

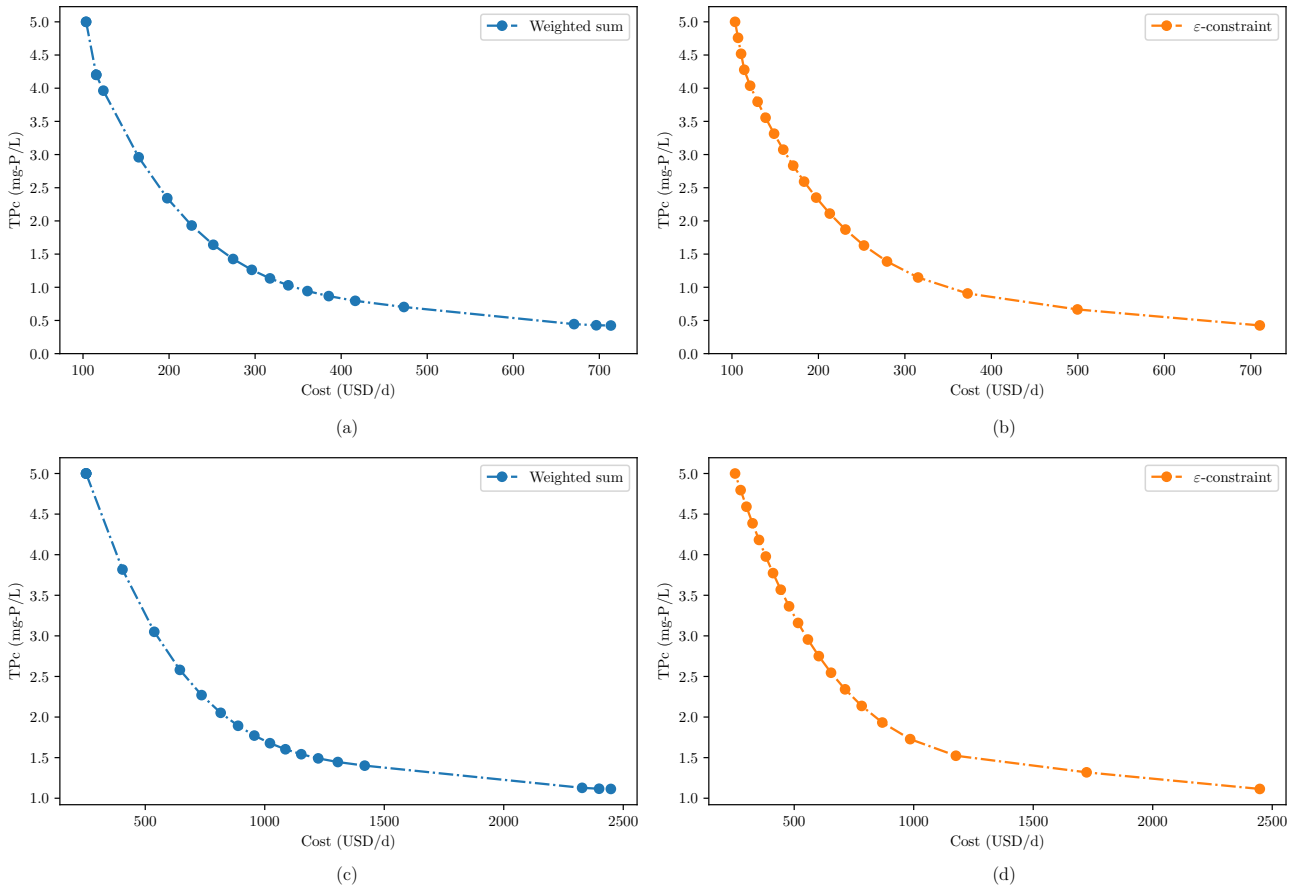

Figure 6. Pareto fronts estimated with the weighted sum and ε-constraint methods for the Al (a-b) and Fe (c-d) scenarios.

Table 5. Performance metrics for the weighted sum and ε-constraint methods used to estimate the Pareto fronts for the Al and Fe scenarios.

	Al Scenario		Fe Scenario	
	Weighted sum	ε-constraint	Weighted sum	ε-constraint
Non-dominated solutions	18	20	17	20
Spacing	194	623	522	2271
Spread	0.49	1.02	0.44	1.03
Hypervolume	2184	2190	6553	6649
Computing time (s)	1.14	1.12	1.18	0.96

4.3. Comparison between precipitating agents

The estimated Pareto fronts offer valuable insights for informed decision-making regarding chemical dosage strategies. In both scenarios, it can be observed from the Pareto fronts (Figure 6) that the cost of phosphorus removal is not proportional to the amount removed, and achieving very low effluent phosphorus concentrations entails a significant increase in operational costs. For instance, in the Al scenario, reducing the effluent phosphorus concentration from the influent value to 5.0 mg−P/L results in a chemical cost of approximately 104 USD/d. Lowering the concentration further to 3.0 mg−P/L increases the cost to 160 USD/d, representing a 54% increase for an additional 40% reduction in phosphorus concentration below 5.0 mg−P/L. Further decreasing it to 1.0 mg−P/L increases the cost to 343 USD/d, which corresponds to a 114% increase from the previous level. This trend is even more pronounced in the Fe scenario: reducing phosphorus to 5.0 mg−P/L results in an estimated cost of 252 USD/d. Lowering it to 3.0 mg−P/L increases the cost to 538 USD/d, and further reduction to 1.0 mg−P/L requires approximately 2450 USD/d, a 355% increase relative to the previous level for the same reduction (2.0 mg−P/L).

It is observed that achieving marginally lower phosphorus concentrations ($TPc \leq 2$ mg−P/L) demands a disproportionately higher investment. Therefore, having the estimation of the Pareto fronts allows plant operators to assess the most cost-effective chemical for different regulatory scenarios. This is particularly valuable if stricter effluent discharge limits are expected in the future, as it helps anticipate which precipitating agent will offer better long-term performance.

For the presented case study, aluminum sulfate appears to be the most cost-effective option across the entire range of phosphorus concentrations. As shown in Figure 7, the Al scenario consistently requires lower metal salt and sodium hydroxide dosages compared to the Fe scenario, and the lower unit cost of aluminum sulfate further contributes to the overall lower cost.

The observed cost differences between aluminum sulfate and ferric chloride could be explained by their distinct effects on system chemistry and dosing requirements. Ferric chloride addition leads to a more pronounced pH reduction due to metal hydrolysis reactions [48], increasing sodium hydroxide demand to maintain optimal pH levels (between 5 and 7 [15]) for efficient phosphorus removal. Moreover, the ferric system typically requires higher molar ratios of metal to phosphorus (approximately 1.6 mol Fe/mol P versus 0.8 mol Al/mol P) to achieve comparable removal efficiencies [49]. As the BioWin model and experimental studies show, ferric removal efficiency decreases at lower pH because H^+ competes with $H_2PO_4^-$ for active adsorption sites [48, 49]. These combined effects lead to higher overall chemical consumption and, consequently, higher operational costs compared to aluminum sul-

fate for this case study.

Although the surrogate model developed in this work is specific to the case-study WWTP and its influent characteristics, the proposed methodology is general and can be applied to other plants and contexts. For each new system, the surrogate model of the corresponding PPR process should be constructed using site-specific data. The construction of the surrogate model can be done using BioWin simulated data or plant operation data if available. If significant influent variability is expected, additional input variables can be incorporated into the surrogate model to capture these effects.

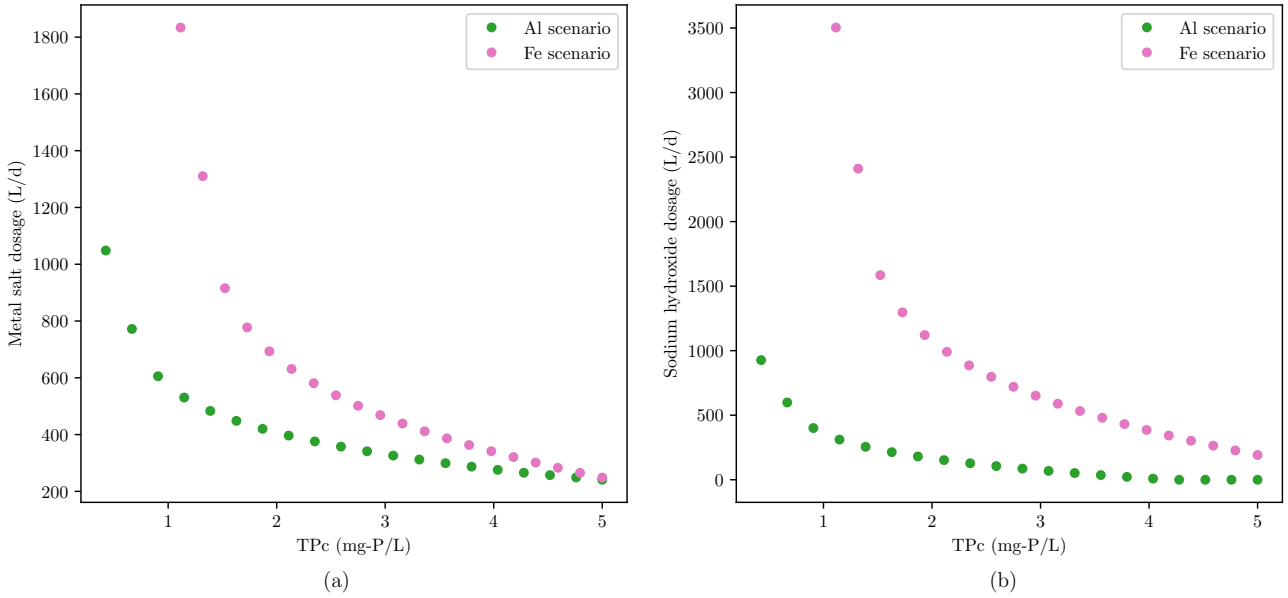

Figure 7. Metal salt (a) and sodium hydroxide (b) dosages against the effluent total phosphorus concentration corresponding to the estimated Pareto fronts for the Al and Fe scenarios.

5. Conclusions

This work proposes a bi-objective optimization framework to analyze the cost-performance trade-off of PPR systems using different precipitating agents. Two commonly employed metal salts, aluminum sulfate and ferric chloride, were compared, using an edible oil WWTP as a case study. The resulting Pareto fronts show the trade-off between phosphorus removal efficiency and operational cost, a critical aspect for WWTPs facing increasingly stringent phosphorus discharge limits. By mapping the effluent phosphorus concentration against costs, the bi-objective approach offers decision-makers insights into how tighter regulations may affect chemical dosing expenses.

Surrogate models enabled the integration of BioWin PPR models into the optimization problem formulation. Polynomial regression models successfully captured the relationship between chemical dosages and effluent characteristics, achieving high predictive accuracy ($R^2 = 0.99$ for both phosphorus and pH). The combination of the weighted sum and ε-constraint methods produced complementary Pareto fronts, offering flexibility to explore different operational trade-offs depending on the decision-maker's objectives. Computational times were consistently short (approximately 1 s), indicating that solution time is not a limiting factor in this problem.

For the edible-oil WWTP case study, aluminum sulfate outperformed ferric chloride in terms of cost-effectiveness, requiring lower metal salt and sodium hydroxide dosages to achieve similar phosphorus removal. While the surrogate model developed is specific to the studied WWTP, the methodology is general and can be applied to other plants.

Overall, the proposed bi-objective optimization approach couples simulation data with mathematical optimization, providing a systematic approach to guide chemical dosing strategies in PPR systems. The framework supports more informed and adaptive operational decisions, helping WWTPs anticipate and manage the economic implications of stricter phosphorus discharge regulations.

Variables

Symbol	Description	Unit
α	Unit cost of metal salt	USD/L
β	Unit cost of sodium hydroxide	USD/L
C	Operational costs	USD/d
C_{anti}	Costs anti-ideal value	USD/d
C_{ideal}	Costs ideal value	USD/d
$Error_{TPc}$	Surrogate model validation error for phosphorus concentration	-
$Error_{pH}$	Surrogate model validation error for pH	-
d_i	Minimal distance between consecutive solutions	-
$\bar{d}$	Average distance between consecutive solutions	-
d_k^e	Distance between a non-dominated solution and nearest extreme point for the k-th objective	-
ε_k	Upper/lower bound ε-constraint method for the k-th objective	-
m	Number of non-dominated solutions	-
OF	Number of objective functions	-
TPc	Phosphorus concentration at the outlet of the PPR system predicted with the surrogate model	mg−P/L
TPc_{BioWin}	Phosphorus concentration at the outlet of the PPR system predicted with BioWin	mg−P/L
TPc_{anti}	Phosphorus anti-ideal value	mg−P/L
TPc_{ideal}	Phosphorus ideal value	mg−P/L
pH	pH at the outlet of the PPR system predicted with the surrogate model	-
pH_{BioWin}	pH at the outlet of the PPR system predicted with BioWin	-
w_k	Weighting coefficient of the weighted sum method	-
x_1	Metal salt dosage	L/d
x_2	Sodium hydroxide dosage	L/d

Use of AI tools declaration

The authors declare they have not used Artificial Intelligence (AI) tools in the creation of this article.

Acknowledgments

The authors would like to express their gratitude to COUSA for providing the data used in this study for academic purposes, especially to Engineers Yamandú Rodríguez, Aldo Giosa, and Felipe Rotondo. Part of this work was financially supported by Comisión Académica de Posgrado (CAP).

Conflict of interest

The authors declare there is no conflict of interest. Diego Rossit is an special issue editor for *Mathematical Biosciences and Engineering* and was not involved in the editorial review or the decision to publish this article. All authors declare that there are no competing interests

References

1. P. Zheng, H. Wang, Z. Sang, R. Y. Zhong, Y. Liu, C. Liu, et al., Smart manufacturing systems for industry 4.0: Conceptual framework, scenarios, and future perspectives, *Front. Mechan. Eng.*, **13** (2018), 137—150. https://doi.org/10.1007/s11465-018-0499-5
2. E. Oztemel, S. Gursev, Literature review of industry 4.0 and related technologies, *J. Intell. Manuf.*, **31** (2020), 127–182. https://doi.org/10.1007/S10845-018-1433-8
3. M. Breque, L. De Nul, A. Petridis, Industry 5.0 – Towards a sustainable, human-centric and resilient European industry, Directorate-General for Research and Innovation of the European Commission, 2021. https://doi.org/doi/10.2777/308407
4. M. Golovianko, V. Terziyan, V. Branytskyi, D. Malyk, Industry 4.0 vs. industry 5.0: Co-existence, transition, or a hybrid, *Proced. Computer Sci.*, **217** (2023),102–113. https://doi.org/10.1016/j.procs.2022.12.206
5. S. Pandey, B. Twala, R. Singh, A. Gehlot, A. Singh, E. Montero, et al., Wastewater treatment with technical intervention inclination towards smart cities, *Sustainability*, **14** (2022), 11563. https://doi.org/10.3390/su141811563
6. United Nations, Goal 6: Ensure access to water and sanitation for all, Available from: `https://www.un.org/sustainabledevelopment/water-and-sanitation/`
7. V. Smith, G. Tilman, J. Nekola, Eutrophication: Impacts of excess nutrient inputs on freshwater, marine, and terrestrial ecosystems, *Environ. Pollut.*, **100** (1999), 179–196. https://doi.org/10.1016/S0269-7491(99)00091-3
8. F. Jiang, M. Beck, R. Cummings, K. Rowles, D. Russell, Estimation of costs of phosphorus removal in wastewater treatment facilities: Construction de novo, *Water Policy Work.*, **10** (2004), 28.

9. R. Bashar, K. Gungor, K. Karthikeyan, P. Barak, Cost effectiveness of phosphorus removal processes in municipal wastewater treatment, *Chemosphere*, **197** (2018), 280–290. https://doi.org/10.1016/j.chemosphere.2017.12.169
10. M. Preisner, M. Smol, Investigating phosphorus loads removed by chemical and biological methods in municipal wastewater treatment plants in poland, *J. Environ. Manag.*, **322** (2022),116058. https://doi.org/10.1016/j.jenvman.2022.116058
11. I. Takács, S. Murthy, P. Fairlamb, Chemical phosphorus removal model based on equilibrium chemistry, *Water Sci. Technol.*, **52** (2005),549–555. https://doi.org/10.2166/wst.2005.0735
12. Metcalf, Eddy, *Wastewater Engineering: Treatment and Resource Recovery*, McGraw-Hill, 5th edition, 2014. ISBN: 978-0-07-340118-8.
13. S. Abdoli, B. Asgari Lajayer, Z. Dehghanian, N. Bagheri, A. H. Vafaei, M. Chamani, et al., A review of the efficiency of phosphorus removal and recovery from wastewater by physicochemical and biological processes: Challenges and opportunities, *Water*, **16** (2024). https://doi.org/10.3390/w16172507
14. J. Bunce, E. Ndam, I. Ofiteru, A. Moore, D. Graham, A review of phosphorus removal technologies and their applicability to small-scale domestic wastewater treatment systems, *Front. Environ. Sci.*, **6** (2018). https://doi.org/10.3389/fenvs.2018.00008
15. A. Szabó, I. Takács, S. Murthy, G. Daigger, I. Licskó, S. Smith, Significance of design and operational variables in chemical phosphorus removal, *Water Environ. Res.*, **80** (2008),407—416. https://doi.org/10.2175/106143008x268498
16. S. Smith, I. Takács, A. Szabo, S. Murthy, G. Daigger, Phosphate complexation model and its implications for chemical phosphorus removal, *Water Environ. Res.*, **80** (2008),428–438. doi.org/10.1002/j.1554-7531.2008.tb00349.x
17. S. Haghiri, A. Daghighi, S. Moharramzadeh, Optimum coagulant forecasting by modeling jar test experiments using anns, *Drink. Water Eng. Sci.*, **11** (2018),1–8. https://doi.org/10.5194/dwes-11-1-2018
18. F. Caro, D. Rossit, C. Santiviago, J. Ferreira, S. Nesmachnow, Multi-objective optimization for the operation of a physicochemical phosphorus removal system, In: S. Nesmachnow, L. Hernández Callejo (Eds.), *Smart Cities*, Springer Nature Switzerland, Cham, 2025, 176–189. ISBN: 978-3-031-85324-1.
19. J. Padrón, S. Almaraz, A. Román, Sustainable wastewater treatment plants design through multiobjective optimization, *Comput. Chem. Eng.*, **140** (2020), 106850. https://doi.org/10.1016/j.compchemeng.2020.106850
20. J. Hakanen, K. Sahlstedt, K. Miettinen, Wastewater treatment plant design and operation under multiple conflicting objective functions, *Environ. Model. Software*, **46** (2013), 240–249. https://doi.org/10.1016/j.envsoft.2013.03.016
21. H.-G. Han, C. Chen, H.-Y. Sun, J.-F. Qiao, Multi-objective integrated optimal control for a wastewater treatment process, *Control Eng. Pract.*, **128** (2022),105296. https://doi.org/10.1016/j.conengprac.2022.105296

22. X. Zhang, S. Yong, Optimization control of wastewater treatment based on neural network and multi-objective optimization algorithm, *Desalin. Water Treatment* **320** (2024), 100736. https://doi.org/10.1016/j.dwt.2024.100736

23. J. Qiao, Y. Hou, H. Han, Optimal control for wastewater treatment process based on an adaptive multi-objective differential evolution algorithm, *Neural Comput. Appl.*, **31** (2019),2537–2550. https://doi.org/10.1007/s00521-017-3212-4

24. E. Tejaswini, S. Panjwani, U. Gara, S. Ambati, Multi-objective optimization based controller design for improved wastewater treatment plant operation, *Environ. Technol. Innov.*, **23** (2021),101591. https://doi.org/10.1016/j.eti.2021.101591

25. T. Liu, H. Zhang, J. Wu, W. Liu, Y. Fang, Wastewater treatment process enhancement based on multi-objective optimization and interpretable machine learning, *J. Environ. Manag.*, **364** (2024),121430. https://doi.org/10.1016/j.jenvman.2024.121430

26. K. Miettinen, Nonlinear Multiobjective Optimization, International Series in Operations Research & Management Science, 1 ed., Springer New York, NY, 1998. https://doi.org/10.1007/978-1-4615-5563-6

27. C. A. Coello Coello, G. B. Lamont, D. A. Van Veldhuizen, Evolutionary Algorithms for Solving Multi-Objective Problems, Genetic and Evolutionary Computation, Springer, New York, NY, 2007. https://doi.org/10.1007/978-0-387-36797-2

28. M. Zelany, A concept of compromise solutions and the method of the displaced ideal, *Comput. Oper. Res.*, **1** (1974), 479–496. https://doi.org/10.1016/0305-0548(74)90064-1

29. Y. Zheng, D. Wang, A survey of recommender systems with multi-objective optimization, *Neurocomputing*, **474** (2022), 141–153. https://doi.org/10.1016/j.neucom.2021.11.041

30. M. T. M. Emmerich, A. H. Deutz, A tutorial on multiobjective optimization: Fundamentals and evolutionary methods, *Natural Comput.*, **17** (2018),585–609. https://doi.org/10.1007/s11047-018-9685-y

31. N. Riquelme, C. Von Lücken, B. Baran, Performance metrics in multi-objective optimization, In: 2015 Latin American Computing Conference (CLEI), 2015, 1–11. https://doi.org/10.1109/CLEI.2015.7360024

32. C. Audet, J. Bigeon, D. Cartiera, S. Le Digabel, L. Salomon, Performance indicators in multiobjective optimization, *European J. Operat. Res.*, **292** (2021), 397–422. https://doi.org/https://doi.org/10.1016/j.ejor.2020.11.016

33. J. Branke, K. Deb, K. Miettinen, R. Słowiński, Multiobjective Optimization: Interactive and Evolutionary Approaches, volume **5252** of *Lecture Notes in Computer Science*, Springer Berlin, Heidelberg, 2008. https://doi.org/10.1007/978-3-540-88908-3

34. J. R. Schott, Fault tolerant design using single and multicriteria genetic algorithm optimization, 1995.

35. K. Deb, *Multi-Objective Optimization Using Evolutionary Algorithms*, Wiley Interscience Series in Systems and Optimization. John Wiley & Sons, 2001. ISBN: 9780471873396.

36. Uruguay, Decreto 253/979, 1979. Available from: `www.impo.com.uy/bases/decretos/253-1979`

37. Isusa, 2024. Available from: www.isusa.com.uy/

38. Efice, 2024. Available from: www.efice.uy/

39. EnviroSim Associates Ltd., BioWin 6.3 User Manual, Hamilton, Ontario, 2024.

40. S. Bentancur, C. López-Vázquez, H. García, M. Duarte, D. Travers, D. Brdjanovic, Modelling of a pulp mill wastewater treatment plant for improving its performance on phosphorus removal, *Process Safety Environ. Protect.*, **146** (2021), 208–219. https://doi.org/10.1016/j.psep.2020.08.029

41. H. Awad, M. Mossad, H. Mahanna, M. Foad, M. Gar Alalm, Comparative assessment of different scenarios for upgrading activated sludge wastewater treatment plants in developing countries, *Sci. Total Environ.*, **907** (2024), 168022. https://doi.org/10.1016/j.scitotenv.2023.168022

42. Instituto Uruguayo de Meteorología INUMET, Características climáticas, 2024. Available from: www.inumet.gub.uy/clima/estadisticas-climatologicas/caracteristicas-climaticas#:~:text=El%20campo%20de%20temperaturas%20medias,la%20costa%20atl%C3%A1ntica%20en%20Rocha

43. R. Bowker, H. Stensel, Design Manual for Phosphorous Removal: EPA 625/1 87/001, US EPA, Washington, D.C., 1987.

44. F. Caro, J. Ferreira, E. Castelló, J. C. Pinto, C. Santiviago, Bio2Py: An API for integrating Python with BioWin for enhanced data acquisition in wastewater treatment simulations, *J. Water Process Eng.*, **63** (2024),105426. https://doi.org/10.1016/j.jwpe.2024.105426

45. M. L. Bynum, G. A. Hackebeil, W. E. Hart, C. D. Laird, B. L. Nicholson, J. D. Siirola, et al., Pyomo–optimization modeling in python, **67**, third ed., Springer Science & Business Media, 2021.

46. A. Wächter, L. T. Biegler, On the implementation of an interior-point filter line-search algorithm for large-scale nonlinear programming, *Math. Program.*, **106** (2006), 25–57. https://doi.org/10.1007/s10107-004-0559-y

47. J. Blank, K. Deb, Pymoo: Multi-objective optimization in python, *IEEE Access*, **8** (2020). https://doi.org/10.1109/ACCESS.2020.2990567

48. H. Hauduc, I. Takács, S. Smith, A. Szabo, S. Murthy, G. Daigger, et al., A dynamic physicochemical model for chemical phosphorus removal, *Water Res.*, **73** (2015), 157–170. https://doi.org/10.1016/j.watres.2014.12.053

49. EnviroSim Associates Ltd., BioWin Advantage 10.1: Investigating Chemical Phosphorus Removal in BioWin 6, 2021. Available from: https://envirosim.com/8553